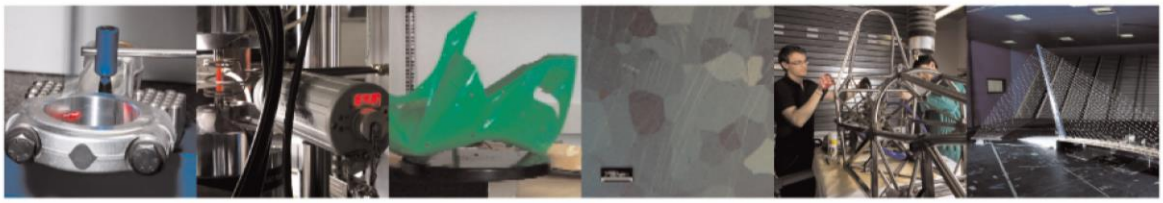

Determining the feasible conditions for processing lunar regolith simulant via laser powder bed fusion

Caprio, L.; Demir, A. G.; Previtali, B.; Colosimo, B. M.

This is a post-peer-review, pre-copyedit version of an article published in ADDITIVE MANUFACTURING. The final authenticated version is available online at:
http://dx.doi.org/10.1016/j.addma.2019.101029

Determining the feasible conditions for processing lunar regolith simulant via Laser Powder Bed Fusion

Leonardo Caprio[1,*], leonardo.caprio@polimi.it

Ali Gökhan Demir[1], aligokhan.demir@polimi.it

Barbara Previtali[1], barbara.previtali@polimi.it

Bianca Maria Colosimo[1], biancamaria.colosimo@polimi.it

[1]Department of Mechanical Engineering, Politecnico di Milano, Via La Masa 1, 20156 Milan, Italy

*Corresponding author

Determining the feasible conditions for processing lunar regolith simulant via Laser Powder Bed Fusion

Leonardo Caprio[1,*], Ali Gökhan Demir[1], Barbara Previtali[1], Bianca Maria Colosimo[1]

[1]Department of Mechanical Engineering, Politecnico di Milano, Via La Masa 1, 20156 Milan, Italy
*Corresponding author

Abstract

Additive manufacturing shows an intrinsic compatibility with building in extra-terrestrial colonization. The use of raw materials found *in situ* can drastically reduce the complexity of the material supply chain. Laser Powder Bed Fusion (LPBF) is a flexible option for producing components starting from powder feedstock. However, further understanding of the technological capabilities is required to resolve both deposition issues and process applicability in space. This work addresses the processability of lunar highlands regolith simulant NU-LHT-2M by Laser Powder Bed Fusion on an open prototypal system. The investigation into the influence of process parameters and different base plate materials (carbon steel, self-supporting deposition and refractory clay) was enabled by the in-house developed LPBF machine. The process feasibility window for multi-layer deposition was determined on the refractory clay base plate which ensured stable deposition. Finally, process parameters were studied to produce multi-layer cubical samples which were further analysed for their mechanical properties. Specimens presented compressive yield stress values in excess of 31.4 MPa and micro hardness values in excess of 680 HV, showing the potential of the technology for the deposition of lunar regolith components. The results were also interpreted to assess the technological feasibility of future LPBF machines which may operate in micro gravity conditions.

Keywords: Laser Powder Bed Fusion, process development, regolith, space manufacturing

1 Introduction

Renewed interest in lunar and spatial exploration has invigorated the development of technologies aimed at more efficient and effective use of the available resources. Additive Manufacturing (AM) processes have been identified as enabling technologies for *in situ* resource utilization (ISRU) during extra-terrestrial investigations[1]. This approach to in-space manufacturing combines the flexibility and design freedom of these novel production routes with the use of local feedstock. With this objective in mind, there has been on-going research within different AM fields. The most notable results have been reported using the D-shape technology, which is a patented binder jetting system whereby successive layers of feedstock power are joined together by means of a liquid binder, whose composition however has not been published[2]. This process is capable of manufacturing building blocks made of lunar regolith simulant JSC–1A which may act as an outer layer of the shelter of future lunar bases, according to studies conducted in collaboration with the European Space Agency (ESA) [1,2].

Most recently, another extrusion-based AM technology has been employed to deposit lunar mare regolith simulant JSC–1A after mixing with an elastomeric binder[3,4]. The technology enables accurate deposition of micro-structures. Still, the availability of the binder may be viewed as limiting when it comes to developing fully autonomous ISRU processes. Alternatively, investigations in literature have focused on the use of solar radiation for the 3D printing of lunar regolith simulant, as carried out by Meurisse *et al.* [5]. Microwave processing of actual lunar soil has been demonstrated by Taylor and Meek [6] and could be used for the construction of roads upon the lunar surface. A successive investigation by Allan *et al.* [7] regarding the microwave processing of JSC-1A shows the potential of the sintering for the realisation of bulk lunar regolith components. Further studies have been conducted by Fateri *et al.* [8] showing the potential of the microwave technology for the sintering of JSC-2A. Schleppi *et al.* [9]

have also been microwave sintering different lunar regolith simulants in order to realise reflective mirrors (through a successive coating of the surface).

Within the industrial panorama, one of the most reliable and promising AM technologies is the Laser Powder Bed Fusion (LPBF) process, which employs a high brilliance laser beam to selectively melt successive layers of powder [10,11]. Although powder bed fusion technologies cannot compete in terms of productivity with binder jetting processes (such as the D-Shape technology), they might be found complementary in terms of the precision and improved mechanical properties of the components produced. Indeed, the minimum feature which may be deposited is closely connected to the dimension of the laser spot size (often in the order of some tens of microns) [12–15]. The application of such a technology is therefore more indicated for producing components whose size is in the millimetre range rather than construction elements. In terms of extra-terrestrial use, LPBF has the advantage of not requiring a binder and potentially working with only the raw material found *in situ*. The lasers employed in most of the common LPBF systems are solid state fibre lasers, which are compact opto-electronic devices. Hence, the direct conversion of electrical power to photons is another advantage reducing the complexity of the production system.

Although there is great potential for the use of LPBF as the key technology for *in situ* resource utilization of lunar regolith, a roadmap to identify the optimum processing conditions with a methodological approach is still required. The first experiments for the deposition of a lunar regolith simulant (JSC–1A) by means of laser based technology were conducted by Krishna Balla *et al.*[16]. The experimental set up was that employed for the AM technology of Directed Energy Deposition. It was not until the work by Fateri and Khosravi [17] that the JSC–1A powder was tested on a LPBF set up. Promising results in terms of component applicability were reported by Fateri *et al.* [18,19] alongside mechanical characterization of the components produced in terms of hardness.

Goulas *et al.* [20] have also been investigating the LPBF of JSC–1A lunar regolith simulant and comparing manufacturability results with martian soil simulants. Among the challenges encountered during the deposition of the material, its low adhesion to the metallic base plate was predominant [21]. The authors therefore developed a proprietary base plate but do not explicitly state its composition. Gerdes *et al.* [22] have also been testing the LPBF technology with basalt powder (which is chemically similar to JSC–1A simulant and Apollo 14 samples of lunar regolith). The authors of the latter work also encountered difficulties in the deposition of the first layers of material and eventually solved them by employing an Al_2O_3 base plate.

The majority of scientific publications have been devoted to the study of JSC–1A powder. It is however important to investigate the processability of different materials since different feedstocks may be employed depending on the region of the Moon where the AM technology may be required. To date, only Abbondanti Sitta and Lavagna [23] have investigated the LPBF of lunar highlands regolith simulant NU–LHT–2M. Nonetheless, details of the technological solutions implemented to overcome initial difficulties and processing instabilities have not been reported. The aim of the present work is to explore the limits and processability issues of depositing NU–LHT–2M lunar regolith simulant by means of Laser Powder Bed Fusion. For this reason, a flexible prototypal system has been employed which allows for flexible variation in the processing conditions, both in terms of base plate and laser parameters. The first part of the research was concerned with the identification of the base plate material which enables the layer wise deposition. Subsequently, process feasibility zones were investigated to identify stable processing conditions whereby multi-layer components could be deposited. Finally, the mechanical properties of the latter in terms of compressive yields stress and Vickers micro hardness are presented. Taking into account the experimental results, there follows a discussion on the applicability of LPBF for space applications. For this purpose, an analytical model to

describe the effects of the main influencing parameters is proposed. Specifically, the modelling allows to evaluate the impact of different gaseous environments and gravitational force on the ejected particulate matter of the laser powder bed fusion process in view of future developments of the technology for in-space manufacturing applications. Finally, the concluding remarks and future developments are presented.

2 Materials and methods

2.1 LPBF system

An open LPBF prototypal system, called Powderful, was employed in the present work. The additive manufacturing system was developed in-house and has been previously employed for different research works since it enables flexible control over process parameters and deposition conditions [24–26]. The laser source incorporated into the prototype system was a single mode fibre laser with a maximum emission power of 250 W (IPG Photonics YLR-150/750-QCW-AC, Cambridge, MA, USA). The divergent laser light from the transport fibre was collimated in the optical chain with a 50 mm focal lens. A moveable zoom optic (VarioScan 20 from Scanlab, Puchheim, Germany) could be employed to regulate the focal position of the laser emission. Beam steering and focusing of the laser light were finally achieved with a scanner head (HurryScan 14 from Scanlab, Puchheim, Germany) equipped with a 420 mm f-theta lens. Theoretical calculations allowed evaluation of the laser beam waist diameter at the focal plane (d_0=60 µm) [27]. Scanning trajectories of the process light were planned using Scanmaster software (Cambridge Technologies, Bedford, MA, USA). The principal parameters of the LPBF system are summarized in Table 1. The design and realisation of the LPBF system Powderful may be viewed in a previous publication by the authors [28] and in the schematic representation of Figure 1. In the configuration of the present work, the powder deposition system consisted in a single hopper for the

storage of the feedstock material. A metallic plate equipped with a piezoelectric transducers acted as a vibration system for the powder delivery allowing powder to flow from the lower slit of the powder hopper. The system allowed to vary the inclination of the metallic plate and its distance from the powder hopper opening, thus enabling flexible regulation of the powder delivered to the powder bed. The powder spreader consisted in an aluminium wiper with a rubber insert that was put in motion by two stepper motors.

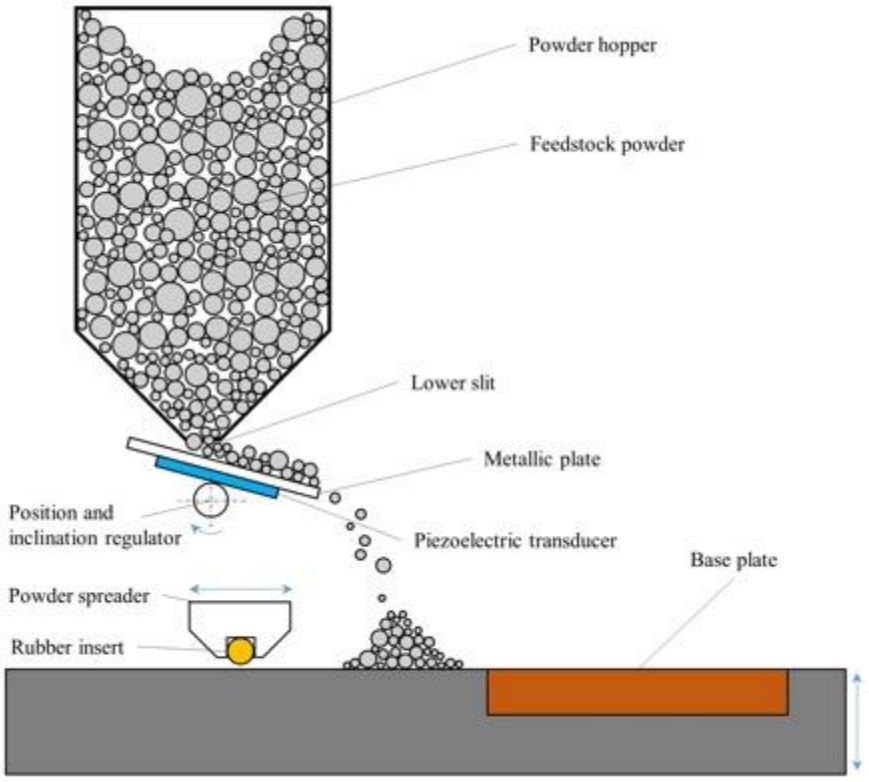

Figure 1. Schematic representation of the powder deposition system (not to scale)

The powder bed and sensors were controlled with LabVIEW programs (National Instruments, Austin, TX, USA). Argon purging was conducted prior to every build by applying a vacuum down to 50 mbar pressure and flooding with Ar gas three times in a row. The system could also be operated in an open atmosphere or with different inertization gases [24].

Table 1. Main specifications of prototypal LPBF system

Parameter	Value
Laser emission wavelength, λ	1070 nm
Max. laser power, P_{max}	250 W
Beam quality factor, M^2	1.1
Beam diameter on focal plane, d_0	60 µm
Build volume (DxWxH)	60x60x20 mm^3

2.2 Lunar regolith simulant and base plate materials

The feedstock material for the powder bed fusion AM process was lunar regolith simulant NU–LHT–2M. The morphology of the powder is reported in Figure 2. The original granulometry of the as-received powder is reported by Abbondanti-Sitta and Lavagna [23]. Excessively large particles were removed from the original batch by manual sieving the powder through a 60 mesh sift. Hence, the particle composition was comprised between 2 and 250 µm. The larger particulate matter was removed in order to improve the flowability of the material. A homogeneous powder layer spreading could be achieved by regulating the powder delivery system of the flexible LPBF prototype.

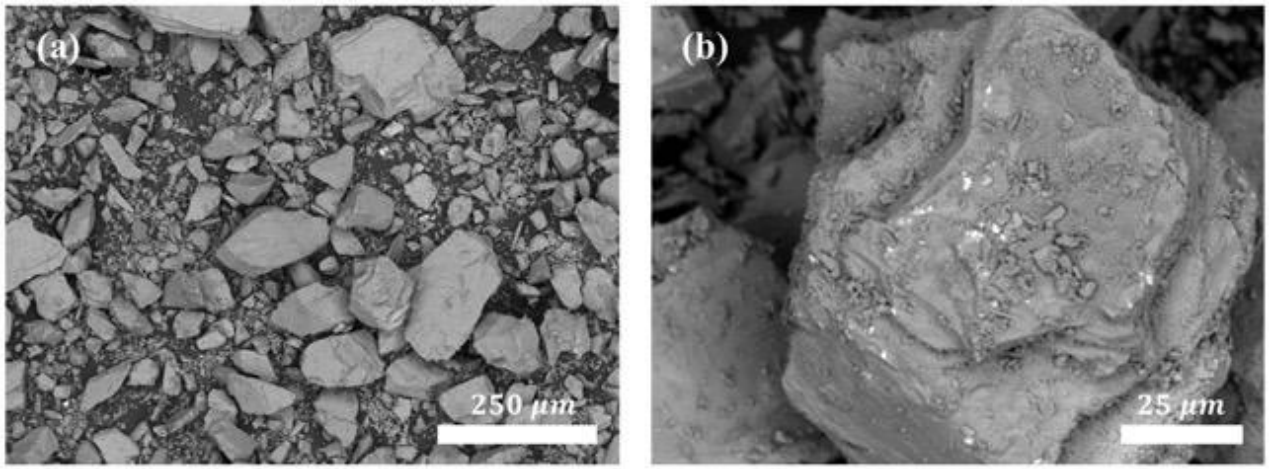

Figure 2. Morphology of regolith simulant NU-LHT-2M captured using SEM with (a) low and (b) high magnifications

The nominal composition of the compounds present in the lunar regolith simulant NU–LHT–2M is shown in Table 2 (as reported on the material safety data sheet and other publications) [29].

Table 2. Nominal composition of compounds of lunar regolith simulant NU-LHT-2M [29]

Compound	SiO_2	TiO_2	Al_2O_3	FeO	MnO	MgO	CaO	Na_2O	K_2O	P_2O_5
wt %	46.7	0.41	24.4	4.16	0.07	7.9	13.6	1.25	0.08	0.15

Two different base plates were used to assess the LPBF of lunar regolith simulant: 12 mm thick C40 steel base plate (chemical composition as defined by standard EN 10277-2:2008[30]) and 12 mm thick refractory clay base plates (Leroy Merlin, Lezennes, France). The chemical composition of the refractory clay was measured by SEM-EDX analysis and compared with the NU–LHT–2M powder (values reported in Table 3).

Table 3. Elemental chemical composition (wt%) of lunar regolith simulant NU–LHT–2M and refractory clay

	Elemental chemical composition (wt%)							
	O	Na	Mg	Al	Si	K	Ca	Fe
NU–LHT–2M	32.87	0.36	2.48	18.21	28.56	-	15.59	1.97
Refractory clay	33.63	-	3.11	12.6	31.69	6.07	4.25	8.65

2.3 Characterization equipment

At an initial phase, the specimens produced were assessed qualitatively through categorical evaluation of the process outcome by means of visual inspection. Scanning electron microscopy imaging and energy-dispersive X-ray (EDX) spectroscopy analysis of base plate material and samples were obtained using a Zeiss EVO 50 XVP (Zeiss, Oberkochen, Germany) system.

Multi-layer specimens were produced and analysed for their mechanical properties via microhardness and compression testing. Vickers microhardness indentation was conducted on one replicate of the final experimental campaign using a VMHT30A system (Leica, Wetzlar, Germany) with a 500 gf load and 15 seconds dwell time. Before the microhardness testing, the samples were mounted in resin and polished to reveal metallographic cross-sections for porosity measurements. Images were

acquired through optical microscopy (Ergolux 200, Leitz, Stuttgart, Germany) and using ImageJ software porosity was evaluated using the following relation:

$$p = \frac{A_{pores}}{A_{tot}} \cdot 100 \quad (1)$$

The compression tests were conducted using a MTS (Turin, Italy) servo-hydraulic machine with a 250kN load cell. Specimens were polished to flatten the surfaces in contact with the hydraulic compression tester. In order to test the material in a condition as close as possible to that of the lunar environment, all the samples were placed in a thermo-vacuum chamber in order to bakeout the material. The bakeout procedure was applied at 0.01 Pa and 105°C for 16 h. This procedure raises the temperature of the samples and exposes them to vacuum in order to remove most of the volatiles trapped inside the object.

2.4 Experimental campaign

The experimental work consisted of three phases. The first step consisted in the identification of the base plate material for the LPBF of lunar regolith simulant. The second stage consisted in definition of the processability window for single and three layer deposition of NU–LHT–2M. Finally, the investigation assessed the multi-layer deposition of samples alongside their mechanical characterisation.

In the first stage, which aimed at determining a base plate material that enables the deposition of lunar regolith simulant, three options were considered: C40 steel, refractory clay and a self-supporting powder bed (i.e. floating deposition). The choice of the C40 steel was to investigate the process feasibility with a common base plate material employed in LPBF. The refractory clay was chosen for its potential chemical compatibility with the deposited material. The self-supporting powder bed which consisted in a 10 mm thick powder bed was investigated as an alternative for avoiding issues of processability as well as for reducing the process chain which requires material removal from the base plate. The first two base

plates were evaluated by attempting to deposit a single layer with a square geometry (5mm x 5mm) with a serpentine hatch scanning strategy. On the other hand, the self-supporting test was conducted using an inside out circular spiral trajectory (outer diameter 4 mm). The choice of the different scanning strategy for the self-supporting deposition was done in order to avoid accelerations and decelerations at the turning points of the rectangular serpentine scan strategy (previously observed through in-process monitoring by Demir *et al.*[31]). These changes in scan speed cause the formation of localised defects as indicated by *Khairallah et al.* [32] and may be considered particularly detrimental for self-supporting depositions due to the increased absorptivity of high thickness powder beds (theoretically predicted by Streek *et al.*[33]). Schematic representation of the selected base plates and scanning strategies are shown in Figure 3.

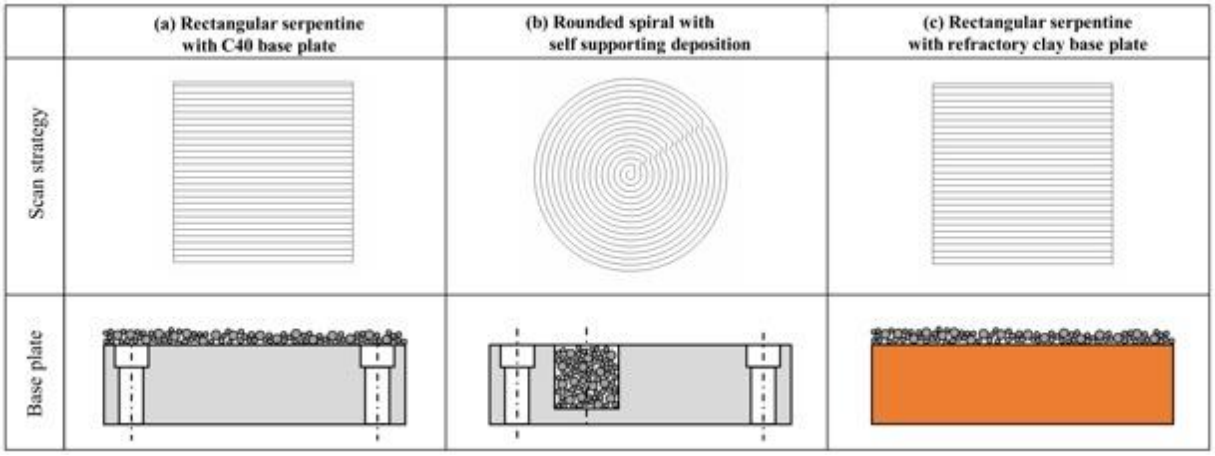

Figure 3. Schematic representation of base plates and scanning strategies tested: (a) Rectangular serpentine with C40 base plate (b) rounded spiral with self-supporting deposition (c) rectangular serpentine with refractory clay base plate. Drawings not to scale.

Experiments were conducted in a closed chamber with inert Ar gas (99.998% purity) in order to avoid contamination by the presence of oxygen and humidity present in the ambient atmosphere. The focal position of the laser beam was kept on the surface of the substrate material and was kept fixed hence the beam waist diameter corresponded to d_0=60 µm. Layer thickness (z) was fixed at 150 µm taking into consideration the model by Zhang *et al.* [34] which allows to estimate the effective layer thickness

during the process. In the hypothesis of a powder bed relative density of 0.5 with respect to the bulk material, the effective layer thickness after a few layers would reach 300 μm thus enabling the deposition of the greater size particles of the powder. The nominal value of layer thickness employed in the work is higher compared to values employed for the LPBF of metallic materials but comparable to values tested by Fateri *et al.* [19] and Goulas *et al.* [21] for the deposition of JSC–1A lunar regolith which have thus been taken as reference for these experimental campaigns.

Hatching distance (h) was maintained at 75 μm. The resultant beam overlap is negative in these conditions. However, due to the fact that the molten pool width is typically greater than the beam waist diameter (as observed through high speed imaging by Bruna-rosso *et al.* [35] and through single track morphological measurements by Yadroitsev *et al.* [36]) it may be expected that overlapping between successive scan tracks will effectively occur. Negative overlap has been shown to produce fully dense components concerning metallic materials in literature[37]. Laser power (P) and scan speed (v_{scan}), were varied in an exploratory way for the deposition on carbon steel and refractory clay base plates (details may be found in Table 4). In order to establish the optimal base plate for the deposition, categorical analysis of the area processed by the laser beam was conducted according to the following categories: inconsistent or no deposition, stable deposition and excessive energy. Inconsistent or no deposition corresponds to the processing condition which results in an incongruous resolidification of the feedstock powder without bonding to the base plate. Stable deposition, on the other hand, is when the process is under control and multilayer processing of the material may be achieved. Excessive energy identifies when the process results in unstable deposition with part protrusion or swelling due to an elevated energy density delivered to the feedstock material.

Table 4. Experimental plans for base plate material identification (single layer campaign)

Fixed parameters			
Process atmosphere		Argon	
Beam waist diameter, d_0 (μm)		60	
Focal position, f (mm)		0	
Hatch distance, h (μm)		75	
Layer thickness, z (μm)		150	
Number of layers		1	
Variable parameters			
Base plate material	C40	Self-supporting	Refractory clay
Power, P (W)	100 – 150 – 200 – 250	175	100 – 175 – 250
Scan speed, v_{scan} (mm/s)	100 – 300 – 500 – 700	400	100 – 400 – 700
Scan strategy	Rectangular serpentine	Rounded spiral	Rectangular serpentine

During the second stage another experimental plan was carried out to assess the process feasibility window. Process parameter variation was investigated once again in terms of laser power and scan speed, whilst keeping the other parameters fixed. A three layer deposition was designed in order to identify the processability region of the material where multi-layer components could be achieved. Using the results of the categorical analysis for single and three layer campaigns on the refractory clay base plate, a processability region for NU–LHT–2M was determined. The overall details of the experimental plans for the process optimisation are reported in Table 5.

Table 5. Details of the experimental plans for process parameter optimisation.

Fixed parameters			
Process atmosphere		Argon	
Base plate material		Refractory clay	
Beam waist diameter, d_0 (μm)		60	
Focal position, f (mm)		0	
Hatch distance, h (μm)		75	
Layer thickness, z (μm)		150	
Variable parameters	Single-layer campaign	Three-layer campaign	Multi-layer deposition
Power, P (W)	100 – 175 – 250	50 – 60 – 70 – 80	50 – 55 – 60 – 65 – 70
Scan speed, v_{scan} (mm/s)	100 – 400 – 700	100 – 150 – 200 – 250	200 – 225 – 250
Replicates, n	1	1	2

Finally, a multi-layer deposition to produce components was conducted. In the feasibility zone, cubical samples with 5x5x5 mm^3 dimensions were produced. The cubical specimens were then tested for Vickers microhardness and compression strength. The results were also assessed in terms of the energy density (E), defined as follows:

$$E = \frac{P}{vhz} \tag{2}$$

All experiments were carried out under Ar. A fan was used to blow away the process debris from the processing zone during the scan periods.

3 Results

3.1 Influence of the base plate type

The first attempt at the LPBF of NU–LHT-2M upon the carbon steel base plate was unsuccessful. Inconsistent deposition of the material could be observed for all experimental conditions (as shown in Figure 4 (a)). Local accumulations of the processed material could be identified by the dark colour in contrast with the base plate material. Independently of the processing condition, it is possible to view that the laser beam interacted with the base plate. Although the powder bed was uniformly spread over the base plate, the highly unstable processing condition induced denudation effects causing direct laser interaction with the base plate thus melting and resolidifying it. The regolith simulant did not bond with the underlying base plate except for some localised depositions which cannot however be considered symptomatic of a stable process.

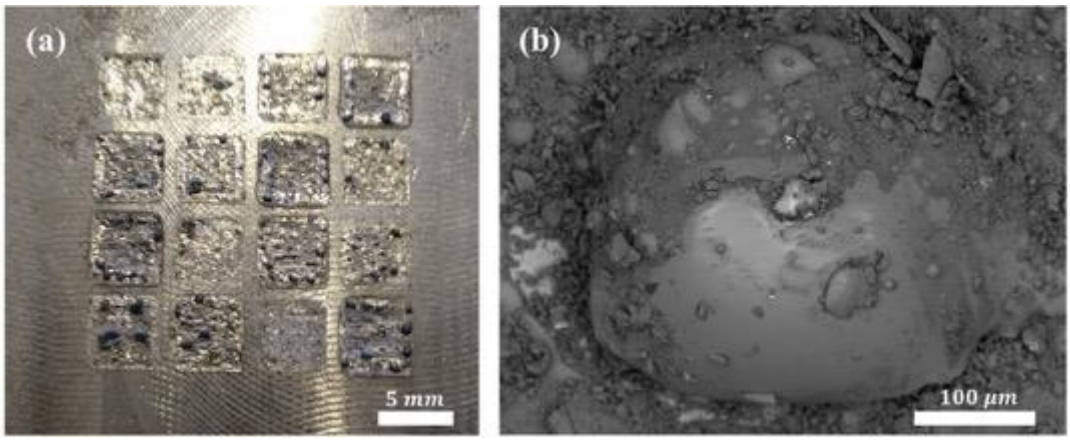

Figure 4. (a) Inconsistent deposition of lunar regolith simulant on carbon steel baseplate after LPBF (b) SEM image of one of the local accumulations.

Closer observation of the inconsistent depositions by scanning electron microscope allows their geometry to be viewed (see Figure 4 (b)). It is possible to view the typical shape of a heterogeneous nucleation process [38]. This is caused by different solidification dynamics between carbon steel and lunar regolith simulant as well as chemical incompatibility between the two.

A further observation related to the single layer deposition was that a consistent presence of particulate matter was observed on the walls of the closed chamber set up at the end of the process. This is indicative of an elevated powder spattering during the process which could be linked to the elevated incompatibility between base plate and powder feedstock. The laser beam interaction with the powder bed in the initial phases of the process caused direct penetration of the beam with the metallic base plate thereby melting the steel (this can be deduced from the heat affected surface shown in Figure 4 (a)). The strong molten pool fluid motion and the generation of localised plume may be interpreted as the main reason for the particle ejection of chemically incompatible powder feedstock.

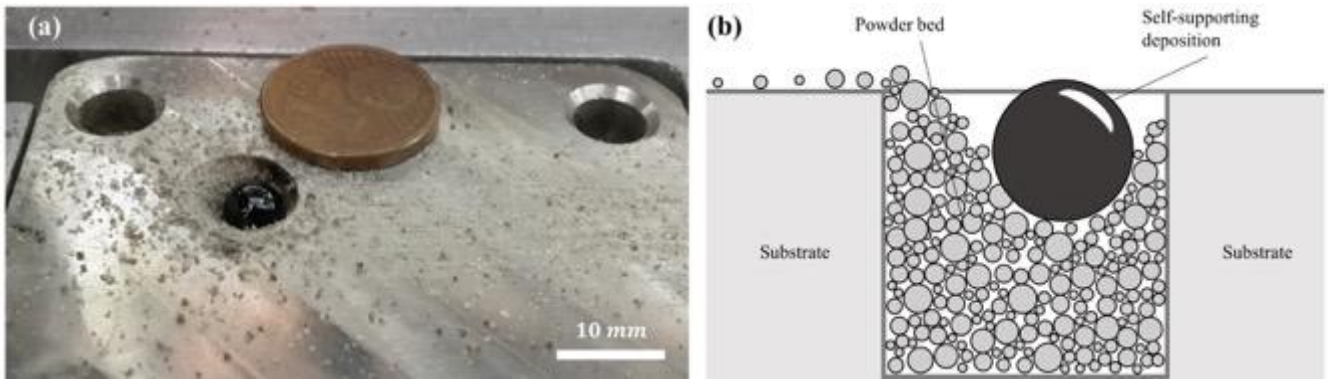

Figure 5. (a) Image of the self-supporting deposition and (b) its schematic representation (not to scale)

The second attempt concerned the self-supporting deposition of NU–LHT–2M on a 10 mm thick powder bed. This experiment was conducted to demonstrate that lunar regolith may be actually melted and resolidified consistently by means of a fibre laser source as well as testing for a different configuration of the base plate. As shown in Figure 5, the feedstock power was reshaped into a single solid component of spherical form. Spattering of neighbouring particles still occurred, probably due to the motion of the molten material. The formation of a spherical shape by the end of the process indicates a weak wetting state between the solid and powder of the regolith simulant probably due to the effect of the Cassie and Baxter effect [39]. When surface tension forces are predominant in liquids, it causes them to assume the shape with the minimum surface energy surface (i.e. a sphere) [40]. The obtained geometry may be better observed in the SEM images of Figure 6, whereby the outer diameter of the sphere was 4.2±0.1 mm.

The contact angle with the lower surface indicates the wettability of the material. Fateri *et al.* observed a high wettability of lunar regolith simulant during the melting process atop of a pre-sintered regolith substrate[41]. The stable formation of the molten pool in LPBF is linked to the physical and chemical properties of the underlying base plate. The carbon steel base plate exhibited differences in thermal conductivity, surface morphology and chemical composition with respect to the feedstock powder. The use of the same material was thus capable of mitigating these differences. This enabled

solidification of the molten material although the low wettability state (probably caused by the geometry of the powder bed which contains the gaseous phase even on the underlying lower contact surface of the melt) indicates the need of a solid surface whereby the material wettability is higher as observed by Fateri *et al.*[41]. These were hence the reasons for testing the third base plate material which consisted of a refractory clay.

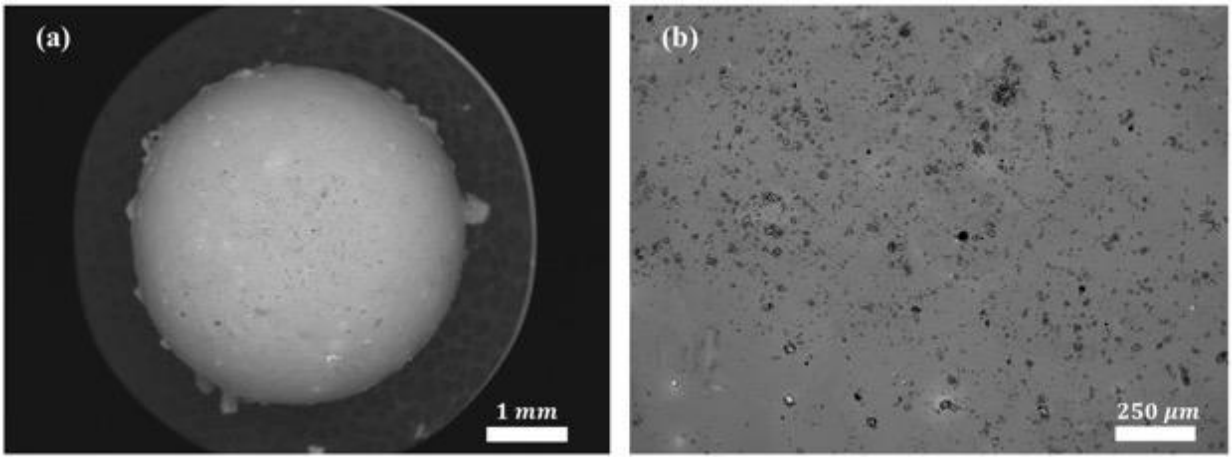

Figure 6. SEM images (a) with low magnification of the self-supporting spherical deposition and (b) high magnification of the top surface of the self supporting deposition

The third test was then conducted upon a refractory clay material that was tested to be chemically very similar to the lunar regolith simulant (Table 3). The process outcome is shown in Figure 7 (a) whilst the categorical analysis is reported in Figure 7 (b). Two major conditions could be identified corresponding to excessive energy and no deposition. Although the material appeared to be processable and was deposited successfully upon the base plate, when the energy input was too high the deposition protruded markedly from the powder bed. As a consequence, the deposition of a second layer of powder was hindered. Excessive energy input could be identified by the formation of pronounced swelling. Figure 7 (a) was acquired straight after the testing of the lunar regolith simulant. It may be viewed that, in the experimental condition, P=250 W and v_{scan}=400 mm/s outgassing, or violent process instability due to vapour formation, disturbed the neighbouring powder bed. This experimental condition was not

the most energetic, yet the outcome was highly unstable. This suggests that the instability during the deposition might be caused by excessive power being delivered to the powder bed causing localised vapour formation rather than allowing stable deposition of the regolith simulant. Unstable deposition with power levels in excess of 50 W had been previously noticed by Krishna Balla *et al.* [16] and it was assumed that the cause for such instability was the low melt viscosity. Accordingly, also Goulas *et al.* [42] and Fateri *et al.* [19] tested lunar regolith simulant with an emission power level of 50 W. Thus, this suggests that there is a threshold value of power beyond which lunar regolith simulant may not be deposited stably (even if the energetic input is regulated by increasing the scan speed). In comparison with ceramic materials typically processed using laser powder bed fusion, which are often susceptible to crack formation due to their weak thermal shock resistance, NU–LHT–2M did not show the presence of cracks on the deposited specimen[43]. Thus, the use of preheating systems which are often employed for the processing of ceramics to reduce thermal gradients and solidification rates[44,45], appears not to be required for the deposition of the lunar regolith simulant. On the other hand, NU–LHT–2M showed a "no deposition" condition with further increases of the scan speed (as visible in Figure 7 in the outcome for v_{scan}=700 mm/s for all levels of power emission). In this condition, only a surface colouring of the base plate material in the process area could be observed, without any deposition of the lunar regolith simulant.

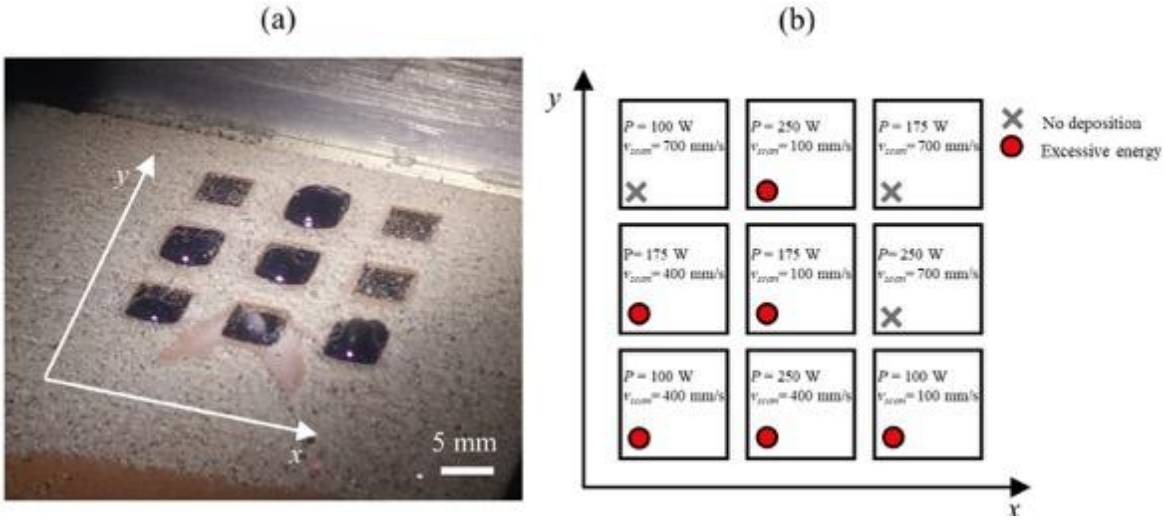

Figure 7. (a) Process outcome of NU-LHT-2M single layer deposition and (b) experimental plan layout with categorical analysis

3.2 Process feasibility zone

Having assessed the refractory clay as the base plate material which enables the deposition of NU–LHT–2M, further experimentation was conducted in order to define the process feasibility zone for the multi-layer deposition of components. Previous results indicated that excessive laser power was being absorbed by the material resulting in unstable deposition. Hence, the second experimental campaign was designed to operate at a lower range of power emission levels (P= 50-80 W) and with scanning speed levels between 100 mm/s and 250 mm/s. The experimental campaign layout and its results are reported in Figure 8.

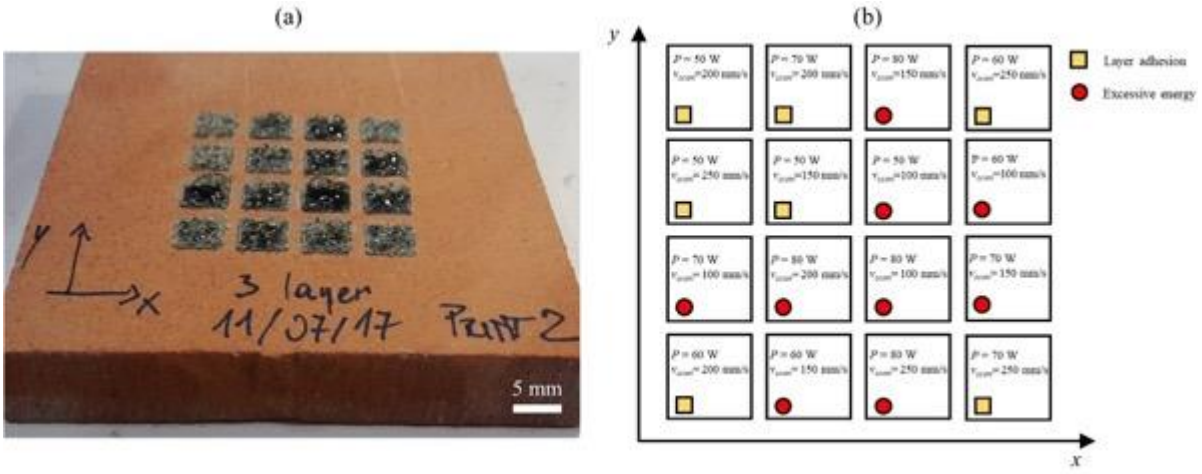

Figure 8. (a) Process outcome of three layer NU-LHT-2M deposition and (b) experimental plan layout and categorical analysis

In order to view the process feasibility area identified through the first two experimental campaigns effectively, it is useful to refer to Figure 9 where the categorical analysis results are reported graphically on a power *vs* scan speed graph. The excessive energy input region, where the process instability conditions were observed, is indicated by the rounded red colour symbols. This area corresponds to conditions where an excessive contribution of energy was deployed either due to high power emission levels or low scanning speed values.

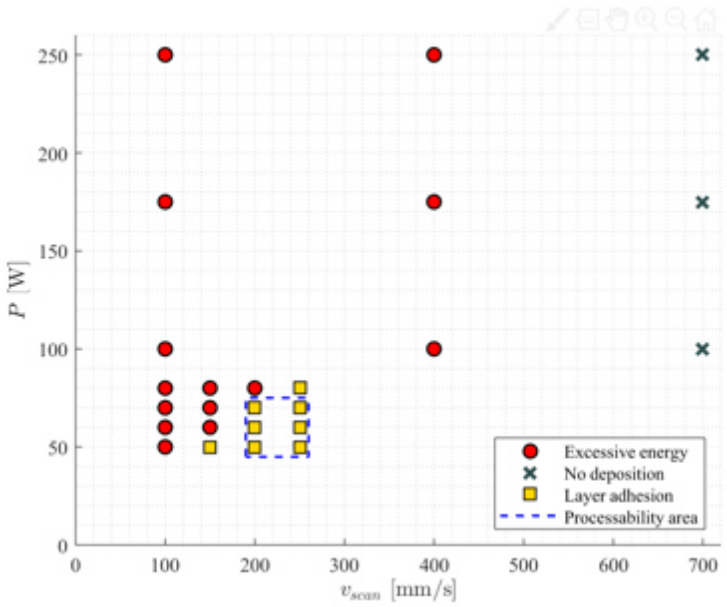

Figure 9. Processability area (blue dashed line) as identified after single layer and three-layer deposition tests. Excessive energy condition indicated with red circle, no deposition with grey cross and layer adhesion with yellow square.

The processability area is demarcated by the dashed blue line of Figure 9 and the final experimental campaign to deposit multi-layer specimens was conducted within this region, testing for 5 levels of power and 3 levels of scan speed. Results were once again analysed by category, indicating conditions in which excessive energy input was employed resulting in unstable multilayer deposition, no deposition conditions due to low intra-layer adhesion and stable deposition conditions where multi-layer components were achieved. Specimen deposition and categorical analysis are reported in Figure 10, showing how the process feasibility area narrows itself down once again.

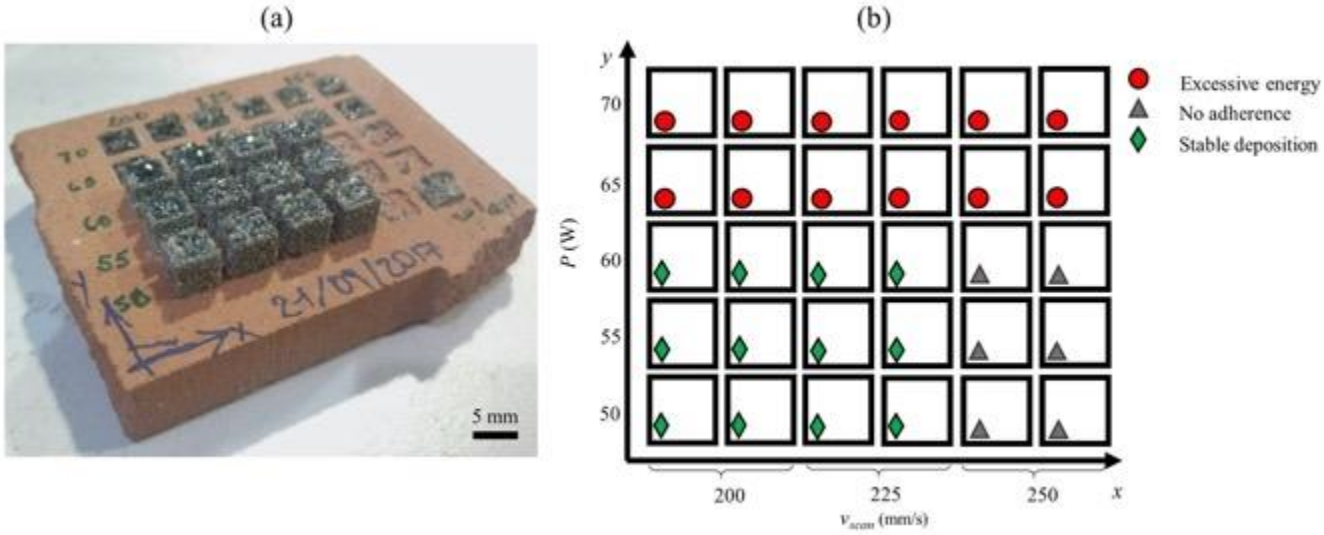

Figure 10. (a) Multi layer regolith simulant specimens deposited by means of LPBF and (b) layout of experimental campaign within processability area. Categorical analysis of process outcome: Excessive energy condition indicated with red circle, no adherence with grey triangle and stable deposition with green rhombus.

The multi layer components were deposited using laser emission power ranging from 50 W to 60 W and with 200 and 225 mm/s scan speed. With respect to industrial parameter for ceramic materials (such as Al_2O_3/ZrO_2), these values of energy density are smaller by an order of magnitude [46].

3.3 Material characteristics

Porosity of the specimen was shown to decrease at lower levels of energy density as reported graphically in Figure 11 although levels are still high in comparison to those of standard LPBF processed materials. Compressive strength results, shown on the secondary axis of Figure 11 appear to have a trend with respect to the energy density parameter, with an increase in yield stress when less energetic process parameters are employed. The highest compressive yield stress (σ_{CYS}= 31.4 MPa) was obtained on the edge of the process feasibility region (P=50 W, v_{scan}=225 mm/s). Thus, for the technology under analysis, the highest mechanical properties were obtained with the highest productivity possible.

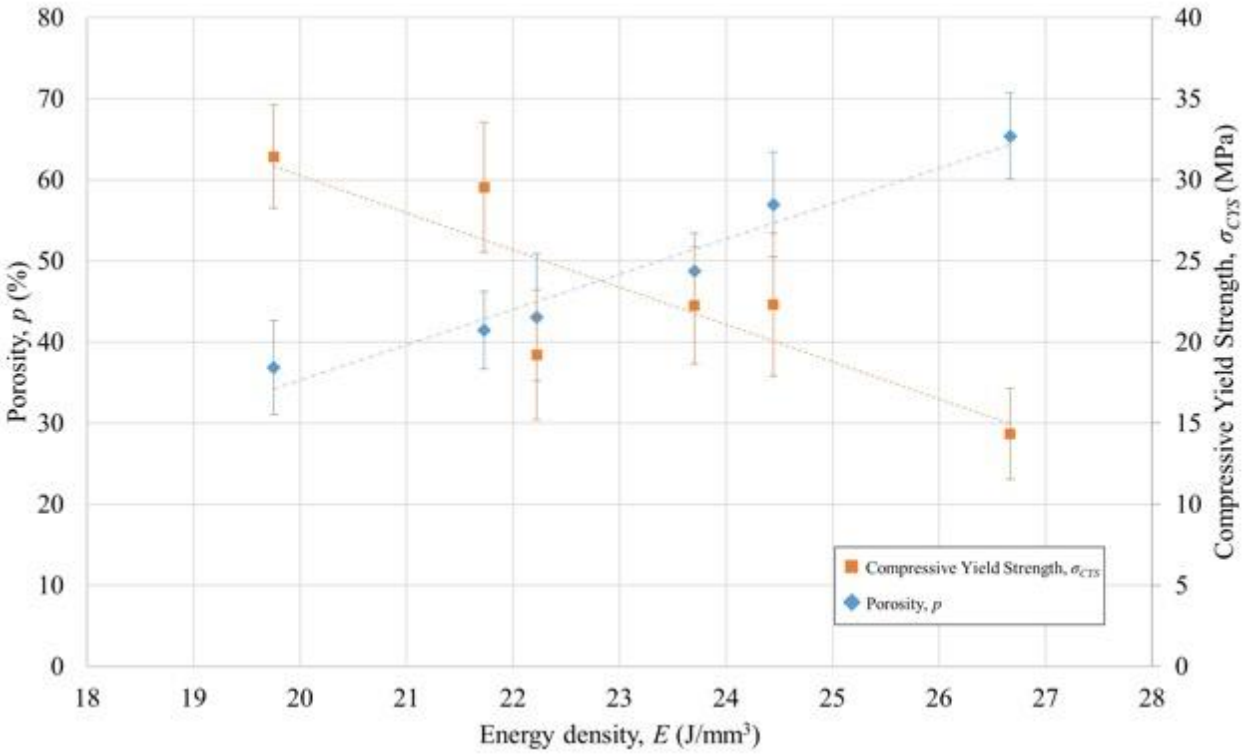

Figure 11. Porosity and compressive yield stress variation against energy density in the process feasibility condition. Error bars report confidence interval of the measurements whilst dashed trend lines are reported on the graphs.

In comparison to existing examples in literature, the values obtained can be considered promising. Table 6 indicates the compressive strength of different lunar resource derived structural materials, their production process and the porosity of the tested specimen if was reported by the authors. Compressive strength is well in excess of the values reported for the Solar 3D printing technology by Meurisse *et al.* [5] (σ_{CYS}=2.3 MPa) and for the D-shape technology by Cesaretti *et al.* [2] (σ_{CYS}=20 MPa). Nonetheless, values in excess of 200 MPa reported by Indyk *et al.* [47] and Gualtieri and Bandyopadhyay [48] for thermally sintered JSC-1A (using conventional sintering method through application of external pressure and heating at elevated temperatures), indicate that there is still a margin for the improvement of the mechanical characteristics of LPBF deposited material. Compression strength testing of samples produced through conventional concrete production process have reported values ranging from 31 MPa (Toutanji *et al.,*[49]), 37 MPa (Montes *et al.*, [50]) to 74 MPa (Lin *et al.* [51]).

Table 6. Compressive strength and corresponding porosity level for various lunar resource derived structural materials (production process is also indicated). nr stands for not reported.

Author	Ref.	Process	Material	Porosity, p (%)	Compressive Yield Strength, σ_{CYS} (MPa)
Indyk et *al.*	[47]	Thermal sintering	JSC-1A	1.4	219
Indyk *et al.*	[47]	Thermal sintering	JSC-1A	11.8	85
Gualtieri and Bandyopadhyay	[48]	Thermal sintering	JSC-1 A, JSC-1AF, JSC-1AC	1	232
Gualtieri and Bandyopadhyay	[48]	Thermal sintering	JSC-1 A, JSC-1AF, JSC-1AC	8	103
Faierson *et al.*	[52]	Geothermite reaction	JSC-1A (67%); Al (33%)	nr	13.8
Montes *et al.*	[50]	Concrete production	Lunamer (JSC-1A)	nr	37
Lin *et al.*	[53]	Concrete production	Lunar soil	nr	74
Toutanji *et al.*	[49]	Concrete production	JSC-1 (65%); Sulfur (35%)	nr	31
Cesaretti *et al.*	[2]	Binder jetting	DNA-1; unknown binder	13	20
Meurisse *et al.*	[5]	Solar 3D Printing	JSC-2A	nr	2
Taylor *et al.*	[4]	Extrusion 3D printing	JSC-1A (74%); PLGA (26%)	55	19
Taylor *et al.*	[4]	Extrusion 3D printing	JSC-1A (74%); PLGA (26%)	63	14
Fateri *et al.*	[8]	Thermal sintering; microwave heat treatment	JSC-2A	13	13

From the literature review and the results reported in Table 6, there appears to be a correlation between the mechanical performance of the materials and their porosity (as shown graphically in Figure 12). This is in accordance with the theory for structural materials which predicts lower compressive strength with increasing porosity levels [54,55]. In their work, Indyk *et al.* [47] showed that also for thermally sintered lunar regolith simulant this trend is valid. As in the case of standard LPBF deposited materials, it is thus important to minimise the porosity of samples in order to improve the mechanical performance of the components. The results from the present work also appear to fit in correctly within this relationship. Compressive strengths in the order of 15-30 MPa achieved through the LPBF process may be sufficient for structural materials on the lunar surface due to the reduced performance required in micro-gravity conditions. Moreover, further experimental investigations within the processability

region of the material may enable to decrease further the porosity levels thus enabling to achieve higher mechanical properties.

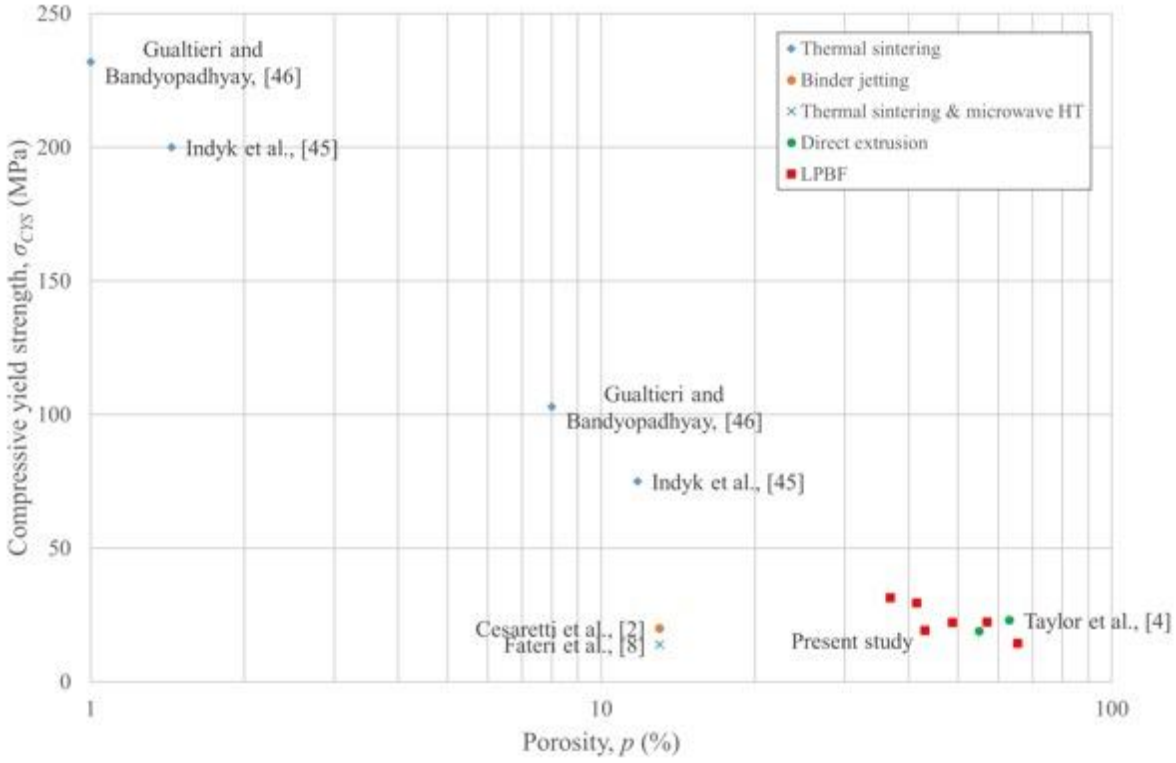

Figure 12. Compressive strength against porosity from values reported in literature. Estimated region of the LPBF process reported in red.

The NU–LHT–2M specimens were also tested for micro hardness as reported in Figure 13. In this case, process parameters did not significantly affect the output variable. The high variability in the measurements is probably due to the varying composition of the specimen being tested and the presence of pores in the components deposited. Values measured are comparable with those reported by Krishna Balla *et al.* [16] (500 HV), Goulas and Friel [21] (670 HV) and Goulas *et al.* (660 HV) [42].

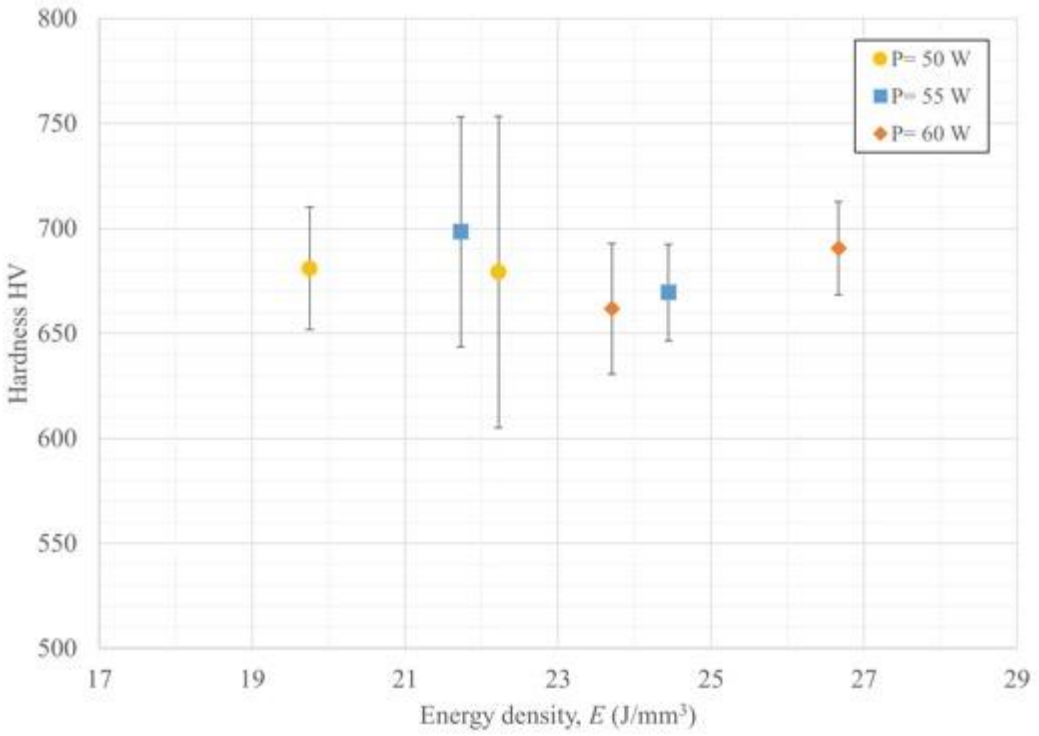

Figure 13. Micro hardness measurement of lunar regolith simulant samples as a function of energy density, *E*. Error bars are one standard error from the mean.

4 Discussion

As evidenced by the experimental results, processing conditions are fundamental to ensure the successful deposition of NU–LHT–2M. Principally, the choice of an opportune base plate is of vital importance to enable the layerwise consolidation of the feedstock powder. An opportunely compatible material should be employed as in the case of refractory clay (chemical similarity to NU–LHT–2M reported in Table 3). Alternatively, ceramic solutions may be experimented as previously demonstrated by Gerdes *et al.*[22]. Considering a future ISRU application, the use of pre-sintered base plates of the same feedstock material could also be a valid alternative.

The results also underline that a high power laser source is not required and is actually disadvantageous for the stability of the process. Apparently, the low thermal conductivity and viscosity of the material render the processing condition feasible in a small range of laser power. This can open up

several possibilities in terms of employing smaller laser sources in footprint as well as energy consumption.

For the future applicability of the technology for ISRU applications in space it is useful to discuss and model the effect of gravity and processing atmosphere for laser powder bed fusion in different operative environments. These aspects are fundamental for process stability since the build-up of particulate matter within the process chamber can be highly detrimental to the LPBF process due to Rayleigh and/or Mie scattering [56]. Either phenomena may occur during laser material processing. The condition for the occurrence of Mie scattering is the presence of suspended particulate matter which may be caused by particle ejections from the powder bed neighbouring the molten pool and the vaporized ejecta. The second condition requires the particle diameter to be of the same order of magnitude as the wavelength of the incident laser beam (which corresponds to the experimental conditions under examination)[57]. In the present work, the authors noticed significant outgassing of particulate matter during the powder bed fusion of lunar regolith simulant which thus may be detrimental for stable processing conditions. Moreover, the use of a process gas was essential to protect the optical chain from the particulate accumulation.

In order to evaluate how different atmospheric conditions may impact the LPBF process a simplified analytical model to evaluate the free fall of particulate matter is introduced. The aim of the model is to provide an insight to the underlying physical theory governing the process and illustrate the effects of operating in extra-terrestrial atmospheric conditions. This aspect is found to be fundamental for machine and equipment design for the extra-terrestrial missions.

When modelling the free fall time in the Ar atmosphere of a particle, two forces may be taken into consideration: drag force and gravitational pull. The drag force (F_D) may be expressed as:

$$F_D = \frac{3 \cdot \eta \cdot \pi \cdot d_p \cdot v_t}{C_c} \quad (3)$$

Where η is the viscosity of the fluid, d_p the particle diameter, v_t the terminal velocity at which the drag force is balanced by the gravitational pull and g the gravitational acceleration [58]. Gravitational acceleration for earth conditions was taken as 9.81 m/s^2 while for moon it was 1.62 m/s^2 [59,60]. It is possible to define the gravitational force acting on a single particle as:

$$F_g = \frac{(\rho_p - \rho_f) \cdot \pi \cdot d_p^3 \cdot g}{6} \quad (4)$$

Where ρ_p is the particle density, ρ_f the density of the fluid (which may be considered as negligible for a gaseous substance). Thus, the terminal velocity is calculated as:

$$v_t = \frac{C_c \cdot \rho_p \cdot g \cdot d_p^2}{18 \cdot \eta} \quad (5)$$

The viscosity of Argon is $2.23 \cdot 10^{-5}$ Pa s, while ρ_p was considered to be 1712 kg m^{-3} which is an average value between the minimum and maximum value of density for lunar regolith simulant NU–LHT–2M [61]. C_c was considered as constant and equivalent to 1 in all conditions. Hence, it was possible to estimate the settling time (t_{fall}) as:

$$t_{fall} = \frac{h_{fall}}{v_t} \quad (6)$$

where h_{fall} is the average distance to deposit and can be considered to be 200 mm for the prototypal set up employed in the present work.

On the other hand, in the case of a vacuum atmospheric condition, the free fall motion of an object can be assumed as uniformly accelerated motion (as demonstrated by the free fall experiment conducted

by Commander David Scott during the Apollo 15 mission) [62]. If an initial velocity is considered null then the settling time from h_{fall} can be determined as:

$$t_{fall} = \sqrt{\frac{2 \cdot h_{fall}}{g}} \tag{7}$$

In order to compare the effect of different atmospheric conditions and the influence of the ejected particle diameter, the graph of Figure 14 was plotted using the models previously described.

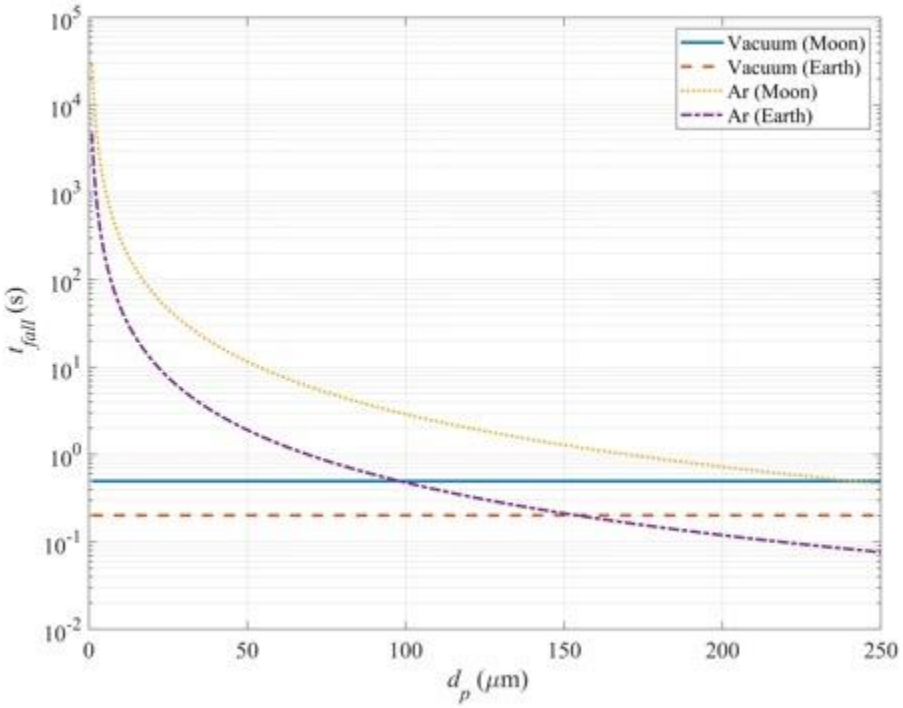

Figure 14. Particle fall time against particle diameter in different atmospheric conditions: blue continuous line for vacuum on the Moon, dashed orange line for vacuum on Earth, dotted yellow line for Ar atmosphere on the Moon and dash-dot line for Ar on Earth

When an Ar atmosphere is considered, the settling time of the particulate matter becomes considerable as the particle diameter decreases both on Earth and on the Moon. As expected, free fall time of particles in vacuum is not influenced by this parameter and generally appears to be substantially lower than t_{fall} when a gaseous substance is present. On the other hand, the ejection of particulate from the processing region in the absence of an atmosphere may be dangerous for the equipment and the

surroundings. Indeed, the nano and micrometric particulate accelerated in vacuum can exceed the speed of sound accelerating the particulate towards space [63,64]. Correct use of an enclosure systems would be essential. Particular attention should be directed to the removal of particles depositing on the optical components of the set up (in a vacuum environment electrostatic forces may become predominant). Alternatively, a strong gas recirculation system should be implemented in order to prevent suspended particle matter from interfering with laser emission. Currently, many industrial LPBF machines are equipped with gas recirculation systems with a two stage filtration system in order to remove the particulate matter from the gas stream in the process chamber. Firstly, a cyclone separator is implemented for the removal of larger particles (due to the higher efficiency of these type of system with greater size particles as stated by Flagan and Seinfeld [58]). Secondly, the gas stream flows through a paper filter which captures the lower size particles. The second stage filter has a finite lifetime which often requires waste disposal at the end of a build process. In order to maximise the lifetime of the paper filter stage (or possibly remove it) a different filtration method may be implemented in extra-terrestial conditions. For instance, in low gravity and low pressure environment, taking into account the greater predominance of electrostatic forces, an electrostatic precipitation system may be equipped. Moreover, the efficiency of the first stage cyclone separator should be further improved by the tendency of electrostatically charged particles to form clusters.

The process feasibility zone currently identified will be influenced by the atmospheric condition under which the powder bed fusion is being conducted [65]. Hence, another optimisation campaign might be required before multi-layer components can be created in extra-terrestrial environment or in a different environment. Nonetheless, the use of low laser emission power is of paramount importance in order to obtain multiple layer deposition without instabilities. This is highlighted by the unfeasibility region beyond 60 W of emission power determined during the experimental campaigns. Nonetheless, this should

not be regarded as a detrimental aspect since, for space applications, a low energy consumption is valuable. Theoretical build rate (*BR*) can be estimated as a function of process parameters as:

$$BR = v_{scan} \cdot h \cdot z \tag{8}$$

In the most productive condition, the build rate for lunar regolith corresponds to 9.11 cm^3/h which is comparable to values of industrially established materials [66]. Mechanical characteristics in terms of both compressive yield strength and micro hardness are comparable to values reported in literature and thus establish LPBF as a possible ISRU technology for future lunar missions.

5 Conclusions

In this study, the processability of lunar regolith simulant NU–LHT–2M by means of Laser Powder Bed Fusion was assessed. From the perspective of employing *in situ* resource utilisation additive manufacturing systems for space exploration, the current research provides a framework for the development of a tailored LPBF machine. This investigation defines functional materials and machine architecture for multilayer deposition of lunar regolith simulant, the choice of optimal laser processing parameters and discusses the effect of low gravity for future advances in technology. The main results of the present research are as follows:

- Refractory clay was determined as an optimal base plate to support multilayer deposition. Self-supporting deposition, although possible, requires further investigation before it can be employed for the freeform fabrication of objects.
- Process feasibility was investigated at varying levels of laser power and scan speed. The processability region of NU–LHT–2M was defined and multi-layer components were produced.

- As deposited NU–LHT–2M specimens presented compressive yield stress up to 31.4 MPa and micro hardness values in excess of 680 HV.
- Taking into account experimental observations and results, alongside considerations on the atmospheric conditions, the optimal deposition framework is discussed for future ISRU applications.

Future studies will attempt to investigate the deposition of the lunar regolith simulant on industrial hardware with forced gas recirculation and vacuum conditions.

6 Acknowledgements

The authors gratefully acknowledge the support of IPG Photonics Italy, Optoprim Srl and Renishaw Italy for contributing the hardware of the experimental set up. This research was partially funded by ASI (Agenzia Spaziale Italiana) within the project ASI-POLIMI on Additive Manufacturing for Space Applications.

7 References

[1] T. Ghidini, Materials for space exploration and settlement, Nat. Mater. 17 (2018). doi:10.1038/s41563-018-0184-4.

[2] G. Cesaretti, E. Dini, X. De Kestelier, V. Colla, L. Pambaguian, Building components for an outpost on the Lunar soil by means of a novel 3D printing technology, Acta Astronaut. 93 (2014) 430–450. doi:10.1016/j.actaastro.2013.07.034.

[3] A.E. Jakus, K.D. Koube, N.R. Geisendorfer, R.N. Shah, Robust and Elastic Lunar and Martian Structures from 3D-Printed Regolith Inks, Sci. Rep. 7 (2017) 1–8. doi:10.1038/srep44931.

[4] S.L. Taylor, A.E. Jakus, K.D. Koube, A.J. Ibeh, N.R. Geisendorfer, R.N. Shah, D.C. Dunand, Sintering of micro-trusses created by extrusion-3D-printing of lunar regolith inks, Acta Astronaut. 143 (2018) 1–8. doi:10.1016/j.actaastro.2017.11.005.

[5] A. Meurisse, A. Makaya, C. Willsch, M. Sperl, Solar 3D printing of lunar regolith, Acta Astronaut. 152 (2018) 800–810. doi:10.1016/j.actaastro.2018.06.063.

[6] L.A. Taylor, T.T. Meek, Microwave sintering of lunar soil: Properties, theory, and practice, J. Aerosp. Eng. 18 (2005) 188–196. doi:10.1061/(ASCE)0893-1321(2005)18:3(188).

[7] S. Allan, J. Braunstein, I. Baranova, N. Vandervoort, M. Fall, H. Shulman, Computational modeling and experimental microwave processing of JSC-1A lunar simulant, J. Aerosp. Eng. 26 (2013) 143–151. doi:10.1061/(ASCE)AS.1943-5525.0000245.

[8] M. Fateri, A. Cowley, M. Kolbe, O. Garcia, M. Sperl, S. Cristoforetti, Localized Microwave Thermal Posttreatment of Sintered Samples of Lunar Simulant, J. Aerosp. Eng. 32 (2019) 1–7. doi:10.1061/(ASCE)AS.1943-5525.0001039.

[9] J. Schleppi, J. Gibbons, A. Groetsch, J. Buckman, A. Cowley, N. Bennett, Manufacture of glass and mirrors from lunar regolith simulant, J. Mater. Sci. 54 (2019) 3726–3747. doi:10.1007/s10853-018-3101-y.

[10] M. Schmidt, M. Merklein, D. Bourell, D. Dimitrov, T. Hausotte, K. Wegener, L. Overmeyer, F. Vollertsen, G.N. Levy, Laser based additive manufacturing in industry and academia, CIRP Ann. 66 (2017) 561–583. doi:10.1016/j.cirp.2017.05.011.

[11] C.Y. Yap, C.K. Chua, Z.L. Dong, Z.H. Liu, D.Q. Zhang, L.E. Loh, S.L. Sing, Review of selective laser melting: Materials and applications, Appl. Phys. Rev. 2 (2015). doi:10.1063/1.4935926.

[12] I. Yadroitsev, A. Gusarov, I. Yadroitsava, I. Smurov, Single track formation in selective laser melting of metal powders, J. Mater. Process. Technol. 210 (2010) 1624–1631. doi:10.1016/j.jmatprotec.2010.05.010.

[13] I. Yadroitsev, I. Shishkovsky, P. Bertrand, I. Smurov, Manufacturing of fine-structured 3D porous filter elements by selective laser melting, Appl. Surf. Sci. 255 (2009) 5523–5527. doi:10.1016/j.apsusc.2008.07.154.

[14] L. Caprio, A.G. Demir, B. Previtali, Comparative study between CW and PW emissions in selective laser melting, J. Laser Appl. 30 (2018). doi:10.2351/1.5040631.

[15] A.G. Demir, B. Previtali, Additive manufacturing of cardiovascular CoCr stents by selective laser melting, Mater. Des. 119 (2017) 338–350. doi:10.1016/j.matdes.2017.01.091.

[16] V. Krishna Balla, L.B. Roberson, G.W. O'Connor, S. Trigwell, S. Bose, A. Bandyopadhyay, First demonstration on direct laser fabrication of lunar regolith parts, Rapid Prototyp. J. 18 (2012) 451–457. doi:10.1108/13552541211271992.

[17] M. Fateri, M. Khosravi, On-site additive manufacturing by selective laser melting of composite

objects, Concepts Approaches Mars Explor. (2012) 12–14.

[18] M. Fateri, A. Gebhardt, M. Khosravi, Experimental Investigation of Selective Laser Melting of Lunar Regolith for In-Situ Applications, Vol. 2A Adv. Manuf. (2013) V02AT02A008. doi:10.1115/IMECE2013-64334.

[19] M. Fateri, A. Gebhardt, Process parameters development of Selective Laser Melting of lunar regolith for on-site manufacturing applications, Int. J. Appl. Ceram. Technol. 12 (2015) 46–52. doi:10.1111/ijac.12326.

[20] A. Goulas, J.G.P. Binner, R.A. Harris, R.J. Friel, Assessing extraterrestrial regolith material simulants for in-situ resource utilisation based 3D printing, Appl. Mater. Today. 6 (2017) 54–61. doi:10.1016/j.apmt.2016.11.004.

[21] A. Goulas, R.J. Friel, 3D printing with moondust, Rapid Prototyp. J. 22 (2016) 864–870. doi:10.1108/RPJ-02-2015-0022.

[22] N. Gerdes, L.G. Fokken, S. Linke, S. Kaierle, O. Suttmann, J. Hermsdorf, E. Stoll, C. Trentlage, Selective Laser Melting for processing of regolith in support of a lunar base, J. Laser Appl. 30 (2018) 032018. doi:10.2351/1.5018576.

[23] L. Abbondanti Sitta, M. Lavagna, 3D Printing of Moon Highlands Regolith Simulant, 69th Int. Astronaut. Congr. (2018) 1–7.

[24] A.G. Demir, L. Monguzzi, B. Previtali, Selective laser melting of pure Zn with high density for biodegradable implant manufacturing, Addit. Manuf. 15 (2017) 20–28. doi:10.1016/j.addma.2017.03.004.

[25] L. Caprio, A.G. Demir, B. Previtali, Comparative study between CW and PW emissions in selective laser melting, J. Laser Appl. 30 (2018) 32305. doi:10.2351/1.5040631.

[26] L. Mazzoleni, L. Caprio, M. Pacher, A.G. Demir, B. Previtali, External Illumination Strategies for Melt Pool Geometry Monitoring in SLM, JOM. (2018). doi:10.1007/s11837-018-3209-1.

[27] A.G. Demir, C. De Giorgi, B. Previtali, Design and implementation of a multi-sensor coaxial monitoring system with correction strategies for selective laser melting of a maraging steel, J. Manuf. Sci. Eng. 140 (2017) 1–14. doi:10.1115/1.4038568.

[28] A.G. Demir, B. Previtali, Multi-material selective laser melting of Fe/Al-12Si components, Manuf. Lett. 11 (2017) 8–11. doi:10.1016/j.mfglet.2017.01.002.

[29] C. Schwandt, J.A. Hamilton, D.J. Fray, I.A. Crawford, The production of oxygen and metal from lunar regolith, Planet. Space Sci. 74 (2012) 49–56. doi:10.1016/j.pss.2012.06.011.

[30] BSI, Bright steel products - Technical delivery conditions, Part 2 Steels Gen. Eng. Purp. BS EN 1027 (2008). papers3://publication/uuid/7427A7C4-516B-416D-A98B-8DB84C66D369.

[31] A.G. Demir, L. Mazzoleni, L. Caprio, M. Pacher, B. Previtali, Complementary use of pulsed and continuous wave emission modes to stabilize melt pool geometry in laser powder bed fusion, Opt. Laser Technol. 113 (2019). doi:10.1016/j.optlastec.2018.12.005.

[32] S.A. Khairallah, A.T. Anderson, A. Rubenchik, W.E. King, Laser powder-bed fusion additive manufacturing: Physics of complex melt flow and formation mechanisms of pores, spatter, and denudation zones, Acta Mater. 108 (2016) 36–45. doi:10.1016/j.actamat.2016.02.014.

[33] A. Streek, P. Regenfuss, H. Exner, Fundamentals of energy conversion and dissipation in powder layers during laser micro sintering, Phys. Procedia. 41 (2013) 858–869. doi:10.1016/j.phpro.2013.03.159.

[34] D. Zhang, Q. Cai, J. Liu, R. Li, A powder shrinkage model for describing real layer thickness during selective laser melting process, Adv. Mater. Res. 97–101 (2010) 3820–3823.

doi:10.4028/www.scientific.net/AMR.97-101.3820.

[35] C. Bruna-rosso, A.G. Demir, B. Previtali, Selective laser melting finite element modeling : Validation with high-speed imaging and lack of fusion defects prediction, Mater. Des. 156 (2018) 143–153. doi:10.1016/j.matdes.2018.06.037.

[36] I. Yadroitsev, P. Krakhmalev, I. Yadroitsava, S. Johansson, I. Smurov, Energy input effect on morphology and microstructure of selective laser melting single track from metallic powder, J. Mater. Process. Technol. 213 (2013) 606–613. doi:10.1016/j.jmatprotec.2012.11.014.

[37] A.G. Demir, P. Colombo, B. Previtali, From pulsed to continuous wave emission in SLM with contemporary fiber laser sources: effect of temporal and spatial pulse overlap in part quality, Int. J. Adv. Manuf. Technol. 91 (2017) 2701–2714. doi:10.1007/s00170-016-9948-7.

[38] W.D. Callister, D.G. Rethwisch, others, Materials science and engineering: an introduction, John Wiley & Sons New York, 2007.

[39] A.B.D. Cassie, S. Baxter, Wettability of porous surfaces, Trans. Faraday Soc. 40 (1944) 546–551.

[40] B. Massey, Mechanics of fluids, 8th ed., Taylor & Francis, 2013. doi:10.1007/978-1-4614-7422-7_12.

[41] M. Fateri, S. Pitikaris, M. Sperl, Investigation on Wetting and Melting Behavior of Lunar Regolith Simulant for Additive Manufacturing Application, Microgravity Sci. Technol. 31 (2019) 161–167. doi:10.1007/s12217-019-9674-5.

[42] A. Goulas, R.A. Harris, R.J. Friel, Additive manufacturing of physical assets by using ceramic multicomponent extra-terrestrial materials, Addit. Manuf. 10 (2016) 36–42. doi:10.1016/j.addma.2016.02.002.

[43] L. Moniz, Q. Chen, G. Guillemot, M. Bellet, C.A. Gandin, C. Colin, J.D. Bartout, M.H. Berger, Additive manufacturing of an oxide ceramic by laser beam melting—Comparison between finite element simulation and experimental results, J. Mater. Process. Technol. 270 (2019) 106–117. doi:10.1016/j.jmatprotec.2019.02.004.

[44] H. Yves-Christian, W. Jan, M. Wilhelm, W. Konrad, P. Reinhart, Net shaped high performance oxide ceramic parts by Selective Laser Melting, Phys. Procedia. 5 (2010) 587–594. doi:10.1016/j.phpro.2010.08.086.

[45] J. Wilkes, Y.-C. Hagedorn, W. Meiners, K. Wissenbach, Additive manufacturing of ZrO2-Al2O3 ceramic components by selective laser melting, Rapid Prototyp. J. 19 (2013) 51–57.

[46] Y.C. Hagedorn, N. Balachandran, W. Meiners, K. Wissenbach, R. Poprawet, SLM of net-shaped high strength ceramics: New opportunities for producing dental restorations, 22nd Annu. Int. Solid Free. Fabr. Symp. - An Addit. Manuf. Conf. SFF 2011. (2011) 536–546.

[47] S.J. Indyk, H. Benaroya, A structural assessment of unrefined sintered lunar regolith simulant, Acta Astronaut. 140 (2017) 517–536. doi:10.1016/j.actaastro.2017.09.018.

[48] T. Gualtieri, A. Bandyopadhyay, Compressive deformation of porous lunar regolith, Mater. Lett. 143 (2015) 276–278. doi:10.1016/j.matlet.2014.11.153.

[49] H.A. Toutanji, S. Evans, R.N. Grugel, Performance of lunar sulfur concrete in lunar environments, Constr. Build. Mater. 29 (2012) 444–448. doi:10.1016/j.conbuildmat.2011.10.041.

[50] C. Montes, K. Broussard, M. Gongre, N. Simicevic, J. Mejia, J. Tham, E. Allouche, G. Davis, Evaluation of lunar regolith geopolymer binder as a radioactive shielding material for space exploration applications, Adv. Sp. Res. 56 (2015) 1212–1221. doi:10.1016/j.asr.2015.05.044.

[51] H. Love, Physical Properties of Concrete Made with Apollo 16 Lunar Soil Sample, Commer.

Oppor. Sp. (1988) 522–533. doi:10.2514/5.9781600865855.0522.0533.

[52] E.J. Faierson, K. V. Logan, B.K. Stewart, M.P. Hunt, Demonstration of concept for fabrication of lunar physical assets utilizing lunar regolith simulant and a geothermite reaction, Acta Astronaut. 67 (2010) 38–45. doi:10.1016/j.actaastro.2009.12.006.

[53] T.D. Lin, H. Love, D. Stark, Physical properties of concrete made with Apollo 16 lunar soil sample, in: Second Conf. Lunar Bases Sp. Act. 21st Century, United States, 1992: pp. 483–487.

[54] N. Narayanan, K. Ramamurthy, Structure and properties of aerated concrete: A review, Cem. Concr. Compos. 22 (2000) 321–329. doi:10.1016/S0958-9465(00)00016-0.

[55] X. Chen, S. Wu, J. Zhou, Influence of porosity on compressive and tensile strength of cement mortar, Constr. Build. Mater. 40 (2013) 869–874. doi:10.1016/j.conbuildmat.2012.11.072.

[56] W.M. Steen, J. Mazumder, Laser Material Processing, 2010. doi:10.1007/978-1-84996-062-5.

[57] R.P. Donovan, Particle Control for Semiconductor Manufacturing, 1990. doi:10.1201/9780203744307.

[58] R.C. Flagan, J.H. Seinfeld, Fundamentals of air pollution engineering, Courier Corporation, 2012.

[59] C. Hirt, W.E. Featherstone, A 1.5km-resolution gravity field model of the Moon, Earth Planet. Sci. Lett. 329–330 (2012) 22–30. doi:10.1016/j.epsl.2012.02.012.

[60] Comptes rendus des séances de la troisième conférence générale de poids et mesures, 1901.

[61] X. Zeng, C. He, A. Wilkinson, Geotechnical Properties of NT-LHT-2M Lunar Highland Simulant, J. Aerosp. Eng. 23 (2010) 213–218. doi:10.1061/(ASCE)AS.1943-5525.0000026.

[62] J.P. Allen, Apollo 15 Preliminary Science Report, Summary of Scientific Results, 1972.

[63] J.H. Lee, D. Veysset, J.P. Singer, M. Retsch, G. Saini, T. Pezeril, K.A. Nelson, E.L. Thomas, High

strain rate deformation of layered nanocomposites, Nat. Commun. 3 (2012) 1164–1169. doi:10.1038/ncomms2166.

[64] D. Veysset, A.J. Hsieh, S. Kooi, A.A. Maznev, K.A. Masser, K.A. Nelson, Dynamics of supersonic microparticle impact on elastomers revealed by real-time multi-frame imaging, Sci. Rep. 6 (2016) 1–7. doi:10.1038/srep25577.

[65] P. Bidare, I. Bitharas, R.M. Ward, M.M. Attallah, A.J. Moore, Laser powder bed fusion at sub-atmospheric pressures, 131 (2018) 65–72. doi:10.1016/j.ijmachtools.2018.03.007.

[66] L. Caprio, A.G. Demir, B. Previtali, Effect of pulsed and continuous wave emission on the densification behaviour in Selective Laser Melting, Proc. 39th Int. Matador Conf. Adv. Manuf. (2017) 1–7.

8 List of tables

9 List of figures

Excessive energy condition indicated with red circle, no adherence with grey triangle and stable deposition with green rhombus.

Figure 11. (a) Porosity and (b) compressive yield stress variation against energy density in the process feasibility conditions. Dashed trend lines are reported on the graphs.

Figure 12. Compressive strength against porosity from values reported in literature. Estimated region of the LPBF process reported in red.

Figure 13. Micro hardness measurement of lunar regolith simulant samples in different processing conditions. Error bars are one standard deviation from the mean and indicate the measurement variability.

Figure 14. Particle fall time against particle diameter in different atmospheric conditions: blue continuous line for vacuum on the Moon, dashed orange line for vacuum on Earth, dotted yellow line for Ar atmosphere on the Moon and dash-dot line for Ar on Earth